Apparent impedance analysis: A small-signal method for stability analysis of power electronic based systems

Atle Rygg and Marta Molinas

***Abstract*—In this paper a new method for power system stability analysis is introduced. The method is based on injection of a small voltage or current in an arbitrary point of a power system. The apparent impedance is then defined as the ratio between the voltage and current at the injection point. It is shown that the apparent impedance can be used to estimate the eigenvalues of the system that are observable from the injection point. The eigenvalues are obtained by applying system identification techniques to the measured set of apparent impedances. The method is similar to the well established impedance-based stability analysis based on source and load impedance models. However, while the source/load impedance ratio is viewed as the minor-loop gain, the apparent impedance can be viewed as a closed-loop transfer function. It can also be expressed as the parallel connection of the source and load impedance. It is shown in the paper how the system eigenvalues can be extracted based on a set of apparent impedance values. The apparent impedance holds therefore complementary information compared with the existing impedance-based stability analysis. The method can also be used as a tool to validate analytically derived state-space models. In this paper the method is presented as a simulation tool, while further work will extend it to include experimental setups.**

Two case-studies are presented to illustrate the method. 1) A DC-case with a buck converter feeding a constant power load, and 2) a three-phase grid-connected VSC with current controller and PLL. The estimated (apparent) eigenvalues of the studied systems are equal to those obtained from the analytic state-space model.

***Index Terms*—Vector Fitting, State-space modeling, Impedance-based analysis, Power system stability analysis.**

I. Introduction

Stability analysis of power systems is often conducted by small-signal methods. Two branches of small-signal methods exist: impedance-based analysis and state-space analysis. The advantage of state-space analysis is the ability to decompose system dynamics into different oscillation modes, and to assess the stability of each mode by eigenvalues and participation factors. The main drawback of state-space analysis is that detailed information and parameter values for all units in the system are usually required. It is also challenging to analytically derive state-space models for system with moderate to large size. The impedance-based method is an alternative method which decomposes the system into a source and load impedance equivalent [1], [2], [3]. Stability can be analyzed by applying the Nyquist Criterion to the ratio between source and load impedances. The main advantage of the impedance-based method is that stability can be analyzed from measurement/simulations in a single point in the system. Hence, this can be viewed as a black-box approach. In order to perform such analysis, a disturbance or perturbation must normally be injected into the system. A drawback of the impedance-based method is that the stability margin depends on the interface point location, i.e. the point which defines source and load subsystem.

A. Rygg and M. Molinas are with the Department of Engineering Cybernetics, Norwegian University of Science and Technology, Trondheim, Norway, e-mail: atle.rygg@ntnu.no

This paper proposes a new method for stability analysis called the apparent impedance method. The approach is based on measurements in a single point similar to the above mentioned impedance-based analysis. However, instead of obtaining the source and load impedances separately, only the equivalent impedance seen from the injection source must be identified. This impedance is defined as the *apparent impedance* and represents a closed-loop transfer function in the system. Consequently, the system state-space model can be estimated based on sampled values of the apparent impedance. Since this is a closed loop transfer function, the eigenvalues of the estimated state-space model is independent of injection location. Well established system identification tools can be used for the estimation. In this work, the Vector Fitting and Matrix Fitting methods are applied [4].

It is remarked that the term apparent impedance is also used within relaying theory as the impedance seen from the relay. Although the definition is similar, the methodology presented in this paper is unrelated to the relaying application with same name.

The method is integrated with existing impedance-based stability analysis techniques and will provide additional information and visualisation. The following four applications of the method are identified, while additional applications can be identified by further work.

- Estimate the system state-space model when parts of the system are only expressed by numerical data / black-box equivalents
- Validate analytically derived state-space models through eigenvalue-by-eigenvalue comparison
- Extend impedance-based stability analysis to also include eigenvalue plot, this can provide additional information and visualisation.
- Obtain a continuous impedance model from a discrete set of impedance values.

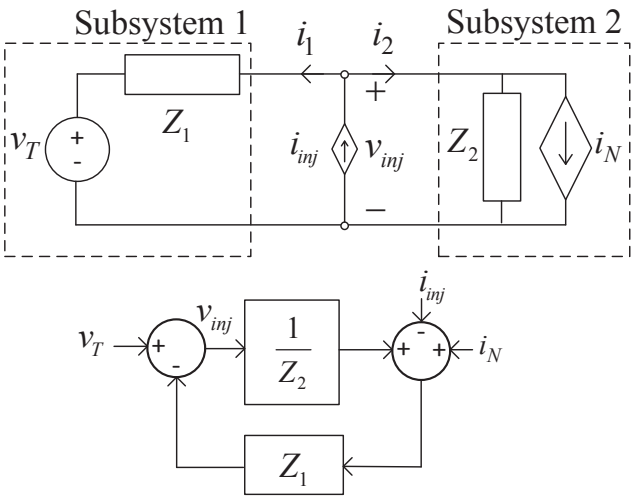

Fig. 1: General DC power system partitioned into two subsystem with shunt injection. Upper: Circuit diagram, lower: Block diagram

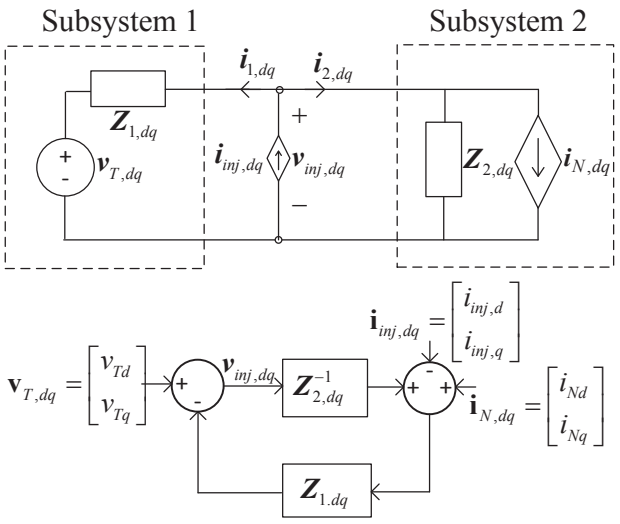

Fig. 2: General three-phase power system in the *dq*-domain with shunt injection. Upper: Circuit diagram, Lower: Block diagram

The presented method will give an accurate validation by comparing each eigenvalue individually, this will also give hints towards where in the modeling the error is located.

The last application is useful when interpreting Bode and Nyquist plots obtained from simulated or measured impedance values. The state-space model obtained from Vector and Matrix fitting methods can be recalculated into a continuous impedance model which will give smooth curves. This will make it easier to accurately identify resonances and to accurately evaluate the behaviour close to the (-1,0)-point in the Nyquist plot.

In this paper the apparent impedance method is presented mainly as a simulation tool. However, it can be extended to also perform online identification of state-space models in experimental setups. Assuming that accurate impedance measurement equipment is available, the implementation will be simple and with low computational requirements.

The paper extends a previous work by the same authors [5]. Here the method was defined for DC-systems, and it was proven that both shunt current and series voltage injection are applicable. Furthermore, a case-study analysis demonstrated that the apparent impedance eigenvalues do not depend on injection location. This paper extends the method to include three-phase systems, and the *dq*-domain is utilized for this task. Only shunt current injection is assumed, but the same results can be obtained by series voltage injection.

II. Apparent impedance definition

The definition of the apparent impedance assumes an injection of voltage or current at some point in the power system. In Fig. 1 an injection is applied to a DC system composed by two subsystems. The injection point separates the system into two subsystems (1 and 2), here represented by their frequency-dependent Thevenin and Norton equivalents.

The apparent impedance is defined as:

$$Z_a(s) = \frac{V_{inj}(s)}{I_{inj}(s)} \tag{1}$$

where V_{inj} and I_{inj} are defined in Fig. 1. Uppercase letters are used to indicate Laplace domain and frequency domain in this paper. The following expressions can then be obtained for Z_a by circuit analysis applied to Fig. 1:

$$Z_a = Z_1 || Z_2 = \frac{Z_1 Z_2}{Z_1 + Z_2} \tag{2}$$

Note that these expressions do not depend on the type of subsystem equivalent (Thevenin vs. Norton) since we are disregarding the impact of the voltage and current sources during small-signal analysis.

III. Stability analysis by the apparent impedance

Apparent impedance stability analysis is a small signal method. The objective is to estimate all eigenvalues of the system based only on sampled values of Z_a. The stability analysis follows directly by evaluating these eigenvalues in the complex plane. A flowchart of the methodology is presented in Fig. 3:

A. DC systems

In small-signal analysis of DC-systems it is assumed that the entire system can be represented by a linearized state-space model:

$$\begin{aligned} s\underline{x} &= A\underline{x} + Bu \\ y &= C\underline{x} + (D + sE)u \end{aligned} \tag{3}$$

where $\underline{x}$ is the vector of n *states*, u is the single input to the system, while y is the single output. A is the $n \times n$ state

matrix, B is a $n \times 1$-vector, C is a $1 \times n$-vector, while D and E are scalars. The term E is required to represent non-proper transfer functions, see section V and appendix B for a related discussion. Note that (3) assumes a Single-Input-Single-Output (SISO) system, which is the case for a DC-system.

In control theory, an impedance represents a transfer function between current and voltage. With reference to the general state-space model (3), the apparent impedance $Z_a(s)$ can be expressed by considering the current i_{inj} as input and the voltage v_{inj} as output in Fig. 1. The Thevenin and Norton sources (v_T and i_N) can be disregarded in this step since they can be viewed as constant under the small-signal assumption. This gives the following state-space model:

$$\begin{aligned} \frac{V_{inj}(s)}{I_{inj}(s)} &= \frac{Z_1 Z_2}{Z_1 + Z_2} = Z_a \qquad (4) \\ sx &= Ax + BI_{inj} \\ V_{inj} &= Cx + DI_{inj} + sEI_{inj} \\ V_{inj} &= (C[sI - A]^{-1}B + D + sE)I_{inj} \\ Z_a &= C\left(sI - A\right)^{-1} B + D + sE \qquad (5) \end{aligned}$$

This is the key point in the derivation process: the apparent impedance represents a closed-loop transfer function in the system. The matrix A will contain the system eigenvalues that are observable from the injection point.

B. Extension to three-phase systems

In this paper the work from [5] is extended to three-phase systems. In this case, the Single-Input-Single-Output (SISO) structure cannot be applied as for DC-systems. State-space modeling in 3-phase systems is often carried out in the *dq*-domain since the variables at fundamental frequency are transformed into constants within this domain [6]-[8]. The zero sequence is normally disregarded, which implies that the system can be represented by 2x2 matrices. Early works and contributions on impedance modeling in the *dq*-domain are e.g. [2],[9]-[12]. More recent contributions can be found in e.g [13] and [14]. The apparent impedance in three-phase systems can be defined by a *2x2* matrix $\mathbf{Z}_{a,dq}$ in the *dq*-domain as:

$$\mathbf{V}_{inj,dq} = \begin{bmatrix} V_{inj,d} \\ V_{inj,q} \end{bmatrix} = \begin{bmatrix} Z_{a,dd} & Z_{a,dq} \\ Z_{a,qd} & Z_{a,qq} \end{bmatrix} \begin{bmatrix} I_{inj,d} \\ I_{inj,q} \end{bmatrix} = \mathbf{Z}_{a,dq}\mathbf{I}_{inj,dq} \qquad (6)$$

By inspecting Fig. 2, the apparent impedance matrix $\mathbf{Z}_{a,dq}$ can be expressed by the subsystem matrices $\mathbf{Z}_{1,dq}$ and $\mathbf{Z}_{2,dq}$ as the parallel connection. The Thevenin source $\mathbf{v}_{T,dq}$ and Norton source $\mathbf{i}_{N,dq}$ can be disregarded due to the small-signal assumption in the same way as in (5). $\mathbf{Z}_{a,dq}$ is the matrix equivalent of (2), and can be derived as follows:

$$\begin{aligned} \mathbf{I}_{inj,dq} &= \mathbf{I}_{1,dq} + \mathbf{I}_{2,dq} \\ \mathbf{I}_{inj,dq} &= \mathbf{Z}_{1,dq}^{-1}\mathbf{V}_{inj,dq} + \mathbf{Z}_{2,dq}^{-1}\mathbf{V}_{inj,dq} \\ \mathbf{V}_{inj,dq} &= (\mathbf{Z}_{1,dq}^{-1} + \mathbf{Z}_{2,dq}^{-1})^{-1}\mathbf{I}_{inj,dq} \\ \mathbf{Z}_{a,dq} &= (\mathbf{Z}_{1,dq}^{-1} + \mathbf{Z}_{2,dq}^{-1}) \qquad (7) \end{aligned}$$

where the last equality is obtained by comparing the third equation with the definition (6). The three-phase system can also be expressed on state-space form by considering the injection current $\mathbf{i}_{inj,dq}$ as input and the injection point voltage $\mathbf{v}_{inj,dq}$ as output:

$$\begin{aligned} sx &= Ax + B\begin{bmatrix} I_{inj,d} \\ I_{inj,q} \end{bmatrix} \\ \begin{bmatrix} V_{inj,d} \\ V_{inj,q} \end{bmatrix} &= Cx + D\begin{bmatrix} I_{inj,d} \\ I_{inj,q} \end{bmatrix} + sE\begin{bmatrix} I_{inj,d} \\ I_{inj,q} \end{bmatrix} \qquad (8) \end{aligned}$$

where A is a *nxn*-matrix, and *n* is the number of states, B has dimension *nx2*, C has dimension *2xn*, while D and E has dimension *2x2*. The state-space model can be reorganized to obtain an expression for the apparent impedance matrix $\mathbf{Z}_{a,dq}$:

$$\begin{bmatrix} V_{inj,d} \\ V_{inj,q} \end{bmatrix} = \left(C\left(sI - A\right)^{-1}B + D + sE\right)\begin{bmatrix} I_{inj,d} \\ I_{inj,q} \end{bmatrix} \qquad (9)$$

$$\mathbf{Z}_{a,dq} = C\left(sI - A\right)^{-1}B + D + sE \qquad (10)$$

where the last equality is obtained by comparing (9) with (6). The matrix equivalent of (5) is then obtained, and can be used as input to the system identification method (matrix fitting). It is then possible to extract the system state-space model and eigenvalues from measured values of the apparent impedance matrix. An example of this method for a grid-connected VSC is included in section VII.

IV. Obtaining apparent impedance from simulations

Obtaining impedance values by simulation can be achieved by most time-domain analysis tools. The idea is to inject a small disturbance in the interface point as illustrated in Fig 1. The disturbance can contain a single frequency (single-tone), or be composed by several frequencies (multi-tone). In this work only multi-tone is applied, but identical results can be obtained by single-tone analysis.

The methodology is illustrated by the flowchart in Fig. 3. Both DC and three-phase systems are considered. The methodology is based on selecting a frequency vector $f_{tab} = [f_1 f_2 ... f_n]$ for which the apparent impedance should be estimated. The next step is to synthesize an injection signal as the sum of sinusoids at these frequencies:

$$i_{inj,DC}(t) = \sum_{i=1}^{n} I_{mag}\sin\left(w_{tab}(i)t\right) \qquad (11)$$

where $\omega_{tab} = 2\pi f_{tab}$.

For three-phase systems, the apparent impedance is a 2x2 matrix in the *dq*-domain. Impedance measurements by frequency sweeps are well established in previous work [15]. Both the *dq*-domain and sequence domain are applied for this task, while the present paper is focusing on the *dq*-domain. A comparison of different injection techniques is out of the scope of this paper, and it is remarked that all techniques will give the same result when the assumption of a Time Invariant (TI) system is satisfied.

The currents and voltages are transformed into the *dq*-domain by applying Park transform with phase angle equal

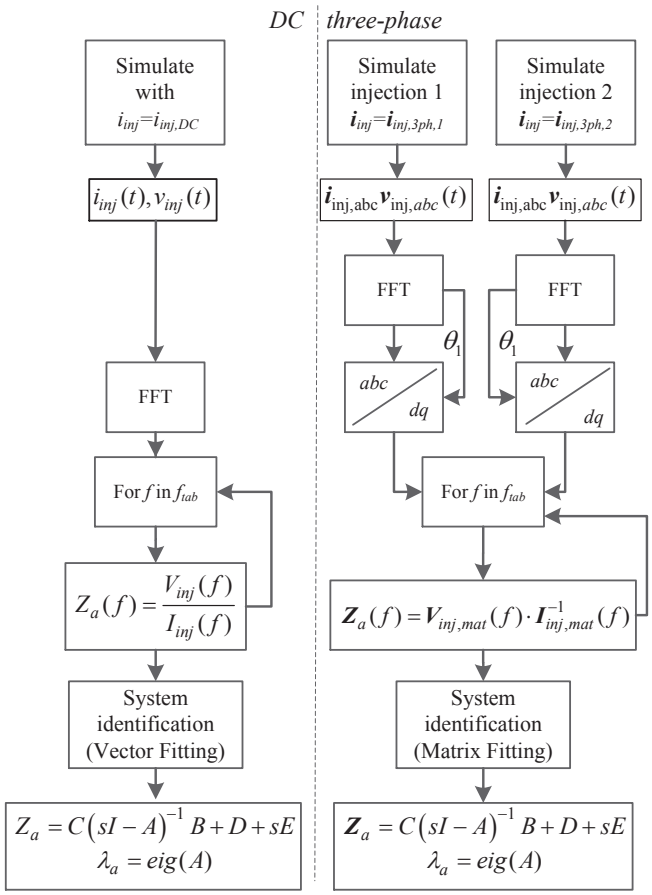

Fig. 3: Illustration of methodologies for obtaining apparent impedances and eigenvalues by numeric simulation with multi-tone injection. Left: DC, Right: Three-phase

to $\theta(t)=\theta_1+\omega_1 t$. The initial condition θ_1 is set equal to the phase A fundamental voltage angle. This angle is identified during post-processing by taking the FFT of the voltage v_{inj}. Consequently, a PLL is not needed to perform the injection. The method for calculating the impedance matrix is based on the work in [15], and it is necessary to combine two linear independent injection signals as explained in [15] and [16]. A possible combination of injection signals is:

$$i_{inj,3ph,1}(t)=\sum_{i=1}^{n} I_{mag}\begin{bmatrix}\sin(\omega_{tab}(i)t)\cos(\omega_1 t+0)\\ \sin(\omega_{tab}(i)t)\cos\left(\omega_1 t-\frac{2\pi}{3}\right)\\ \sin(\omega_{tab}(i)t)\cos\left(\omega_1 t+\frac{2\pi}{3}\right)\end{bmatrix}$$
$$i_{inj,3ph,2}(t)=\sum_{i=1}^{n} I_{mag}\begin{bmatrix}\sin(\omega_{tab}(i)t)\cos(\omega_1 t+0)\\ \sin(\omega_{tab}(i)t)\cos\left(\omega_1 t+\frac{2\pi}{3}\right)\\ \sin(\omega_{tab}(i)t)\cos\left(\omega_1 t-\frac{2\pi}{3}\right)\end{bmatrix} \quad (12)$$

where ω_1 is the fundamental frequency, and the three elements in the vector are the a,b,c phase components. With this choice of injection signals, $i_{inj,3ph,1}$ is a pure d-axis component, while $i_{inj,3ph,2}$ is a pure q-axis component. It is remarked that the injection signals are not synchronized with the grid voltage v_{inj} during simulation, hence the d-axis of the injection signal has an arbitrary phase shift with respect to the grid voltage. Instead, the current and voltage measurements are aligned with the fundamental component of the grid voltage during post-processing. Consequently, the q-axis component of $i_{inj,3ph,1}$ and the d-axis component of $i_{inj,3ph,2}$ will not be zero during post-processing since the d-axis is aligned to a different angle.

The next step is to simulate the system with the above defined injection signals applied ~~to the system~~. Time-domain response of v_{inj} and i_{inj} is then stored and transformed into frequency domain by the Fast Fourier Transform (FFT). For the three-phase case, the responses are transformed to the dq-domain before applying the FFT. The apparent impedance can then be calculated based on the frequency domain data. For the DC-case this is simply the ratio of injection point voltage by injection current (1). For the three-phase case it is necessary to combine the responses from the two injection signals as derived in [15]. The following equation can be used to find the impedance matrix (equation (18) in [15]):

$$\begin{aligned}\mathbf{Z}_{a,dq} &= \begin{bmatrix}V_{inj1,d} & V_{inj2,d}\\ V_{inj1,q} & V_{inj2,q}\end{bmatrix}\begin{bmatrix}I_{inj1,d} & I_{inj2,d}\\ I_{inj1,q} & I_{inj2,q}\end{bmatrix}^{-1}\\ &= \mathbf{V}_{inj,mat}\mathbf{I}^{-1}_{inj,mat}\end{aligned} \quad (13)$$

After this step, the apparent impedance is identified at all frequencies in f_{tab}, and this is the required input data for the system identification process described in the next section.

V. Estimating state-space models by vector fitting and matrix fitting

Vector Fitting (VF) is a well established method for rational approximation in the frequency domain using poles and residues [4] [18] [19]. The method is able to estimate a state-space model to a measured or computed transfer function based on curve fitting. Vector Fitting is widely applied in many engineering fields, from high-voltage power systems to microwave systems and high-speed electronics. A Matlab-implementation of the method is available online [20].

The input to the vector fitting algorithm is:

- A set of measured/simulated apparent impedance values function values $Z_{a1}, Z_{a2}...Z_{an}$ taken at the frequencies $f_1, f_2...f_n$
- The order of the resulting state-space model. The maximum possible value is the number of impedance values (n)

The output of VF is then the state-space model represented by A, B, C, D, E (3). The model is also expressed on pole-residue form, see Appendix C for details.

The fitting algorithm will identify the system eigenvalues with high accuracy when the system under study is time invariant. Still, it must be remarked that the resulting state variables cannot be related to any physical quantities in the system when a pure black-box approach is adopted. This is a consequence of having a black-box approach in general, and not a weakness of the specific method.

Three important options can be selected when running the VF algorithm:

- Stability enforcement

- Passivity enforcement
- Include D and/or E in the fitting

When obtaining the apparent impedance by simulation, it can be assumed that the system is stable. Otherwise, it would not be possible to identify the apparent impedance due to lack of a stable operation point. The stability enforcement can therefore be selected. However, if the apparent impedance is obtained by analytical calculations, e.g. by (2), stability enforcement should *not* be selected.

Generally, it is important to *not* force the system to be passive during fitting. Power electronic converters can inject energy to the system at certain frequencies. Such behavior is the definition of a non-passive system. Passivity enforcement should only be applied in modeling of passive components such as transformers and cables. Recent research is focusing on stability analysis through passivity assessment, see e.g. [21]-[23]. See Appendix E for more information on passivity.

Finally, it is important to include both D and E in the fitting. D is required in order to properly model series resistance in both impedance and admittance models. The physical interpretation of E is a series inductor in an~~d~~ impedance model, and a shunt capacitor in an admittance model. Without the term E, these elements cannot be accurately described by~~on~~ state-space representation.

While VF is applied to SISO-systems, another implementation is able to extract models for MIMO-systems. This is called Matrix Fitting (MF), and is also available online [20]. In this work, VF is applied for DC-systems, while MF is applied for three-phase systems in the *dq*-domain. The above three options can also be selected for MF. In addition the following symmetry condition is enforced by default:

$$\mathbf{Z}_{dq} = \mathbf{Z}_{dq}^{*} \implies Z_{dq} = Z_{qd} \tag{14}$$

where $*$ denotes complex conjugate transpose. This condition is normally *not* met for power electronic systems. Therefore, it has been disabled, allowing each element in the impedance matrix to be independent from the others. More information on matrix fitting can be found in Appendix D.

A. Selecting the model order

An important parameter in the system identification process is the model order. An m'th order model will give *m* states and *m* eigenvalues. The number of states in the system is unknown by the apparent impedance method since this is a black-box approach. A methodology presented in Fig. 4 is proposed to identify insignificant states and eigenvalues. It is known that when the residue R_i divided by eigenvalue λ_i has small absolute value for the state *i*, this state does not contribute to the measured response [4]. Consequently, by gradually reducing model order until all eigenvalues are significant, the correct number of states will be identified. A threshold must also be selected for this detection. In this work, $|\frac{R_i}{\lambda_i}| > 10^{-4}$ is used as a condition for defining λ_i as significant. Note that the initial model order *n* cannot be selected higher than the number of measured apparent impedances.

In case of three-phase system, the residue R_i becomes a 2x2 matrix $\mathbf{R}_{i,dq}$. In order to evaluate the significance of this matrix, it is proposed to use the 2-norm $||\mathbf{R}_{i,dq}||_2$ divided by eigenvalue λ_i. Other matrix norms can also be used.

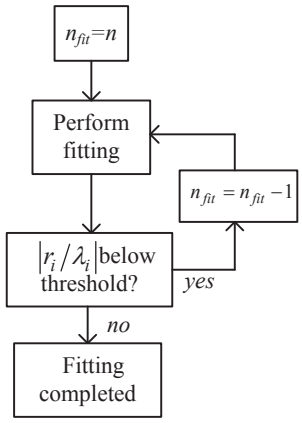

Fig. 4: Illustration of methodology for finding the most suitable model order

It is remarked that the above discussion assumes perfect input data and a fully observable system. In cases where this is not met, the method for selecting model order is also very useful in sorting out eigenvalues that are not estimated with sufficient confidence.

VI. DC CASE STUDY EXAMPLE

A. Case overview: Buck converter feeding CPL

A case study has been defined in Fig. 5. This is a DC-system where a Constant Power Load (CPL) to the right is fed by a Buck converter. The CPL consumes constant power P^* by drawing a current I_L that is inverse proportional to its terminal voltage v_{C2}. The CPL dynamics are represented by the filter time constant τ used to lowpass-filter the measured voltage v_{C2}. The Buck converter has a constant duty cycle D, switching frequency f_{sw} and an output filter represented by R_1, L_1, C_1, R_{c1}. Series impedance R_2, R_3, L_3 separates the source and load from each other. Note that the model is nonlinear due to the term $i_L = \frac{P^*}{\tilde{v}_{C2}^2}$.

The system is represented in *MATLAB Simulink Simscape Power Systems* using a switched (detailed) model. The simulation time step is fixed and equal to $T_{sim} = 1\ \mu s$.

B. Analytical state-space model

By circuit analysis the state-space model of the system in Fig. 5 is derived in (15) - (16). The state-space model is without any elements B, C, D and E since only the eigenvalues of matrix A are relevant for the stability analysis. The CPL has been linearized around its operation point denoted by the stationary voltage V_{C2}. The applied parameter values are given in Table I.

$$s \begin{bmatrix} i_{L1} \\ v_{C1} \\ i_{L2} \\ v_{C2} \\ v_{\tilde{C}2} \end{bmatrix} = A \begin{bmatrix} i_{L1} \\ v_{C1} \\ i_{L2} \\ v_{C2} \\ v_{\tilde{C}2} \end{bmatrix} \tag{15}$$

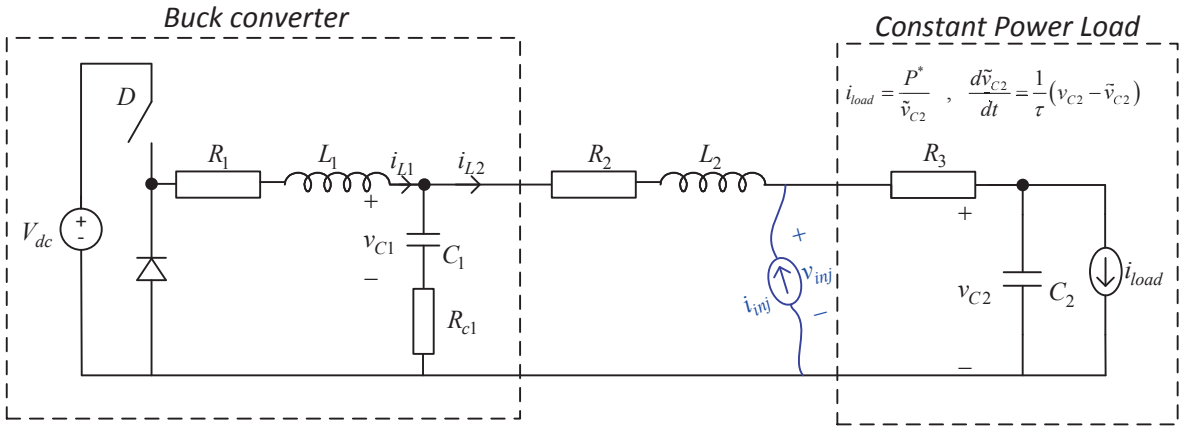

Fig. 5: Schematic of DC case study system, including the injection source (i_{inj})

where

$$A = \begin{bmatrix} -\frac{R_1+R_{c1}}{L_1} & -\frac{1}{L_1} & \frac{R_{c1}}{L_1} & 0 & 0 \\ \frac{1}{C_1} & 0 & -\frac{1}{C_1} & 0 & 0 \\ \frac{R_{c1}}{L_2} & \frac{1}{L} & -\frac{R_1+R_2+R_{c1}}{L_2} & -\frac{1}{L_2} & 0 \\ 0 & 0 & \frac{1}{C_2} & 0 & \frac{P^*}{C_2 V_{C2}^2} \\ 0 & 0 & 0 & \frac{1}{\tau} & -\frac{1}{\tau} \end{bmatrix} \quad (16)$$

TABLE I: Parameter data applied in the simulation model

Parameter	Value	Parameter	Value
V_{DC}	2 V	D	0.5
R_1	10 $m\Omega$	L_1	0.9 mH
C_1	1.1 mF	R_{c1}	500 $m\Omega$
R_2	50 $m\Omega$	R_3	20 $m\Omega$
L_2	1.6 mH	C_2	10 mF
P^*	0.5 W	τ	5 ms.
T_{sim}	1 μs	f_{sw}	2.5 kHz

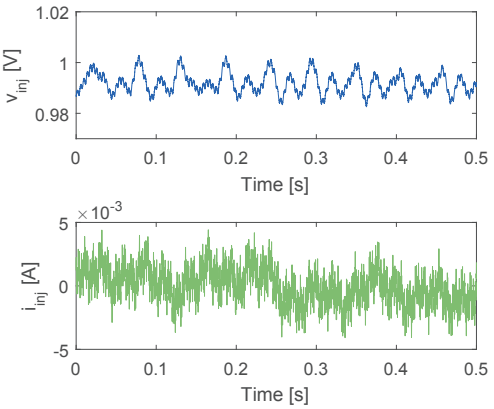

Fig. 6: Steady-state waveforms of i_{inj} and v_{inj}. Injection frequencies given by (17)

The eigenvalues $\lambda_{analytic}$ of the state matrix A have been calculated in MATLAB using the data in Table I. They are compared with the eigenvalues obtained by the proposed method in Section VI-D.

C. Illustration of methodology

In this work, a multi-tone signal composed by 8 frequencies is injected. The frequencies are logarithmically spaced in the range between 2 and 2000 Hz as:

$$f_{tab} = [2, 6, 14, 38, 104, 278, 746, 2000]\ Hz \quad (17)$$

A time-domain simulation of steady-state operation is presented in Fig 6. The injected current i_{inj} as well as the intersection point voltage v_{inj} are indicated in the plot. The amplitude of each injected frequency component is 0.5 mA, giving a total RMS of $\frac{1}{\sqrt{2}} \cdot 8 = 2.8\ mA$. This is approximately 0.5 % of the average load current.

As highlighted in Fig. 3, the signals in Fig. 6 is the *only* information needed to perform the stability analysis. First, FFT is applied to v_{inj} and i_{inj}, and the result is presented in Fig. 7. Since shunt current is applied to this example, the current magnitudes are equal for all injected frequencies, while the voltage depends on the circuit parameters. Apparent impedance is defined in (1) as the ratio between v_{inj} and i_{inj} in the frequency domain.

The resulting impedance plots are presented in Fig. 8. The impedances are estimated for the 8 frequencies in f_{tab}, while the Vector Fitting algorithm is used to obtain the fitted line. Only the impedance magnitudes are presented, but it has been verified that the angles are consistent with the conclusions. The subsystem impedances Z_1 and Z_2 defined in Fig. 1 are also presented in the same plot. They are corresponding to the left (Buck) and right (CPL) subsystem impedances in Fig. 5, respectively.

The impedance plots can be explained as follows: It is clear that the simulated apparent impedance Z_a complies with (2). It represents the parallel connection of the subsystem impedances Z_1 and Z_2. When the two subsystem impedances have large difference in magnitude, $Z_a \approx min[Z_1, Z_2]$. A resonance peak occurs at $f_{max} = 45\ Hz$ where Z_1 and Z_2 have equal amplitude but opposite phase. The angle of Z_a is close to 180 degrees here. At low frequencies, $Z_a \approx Z_1$ since the inductive path through the buck converter has significantly

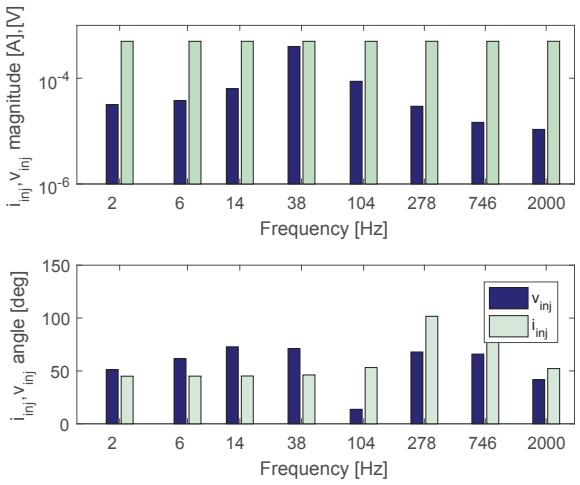

Fig. 7: Harmonic components of i_{inj} and v_{inj} with injection at f_{tab} (17). Obtained by FFT applied to Fig. 6

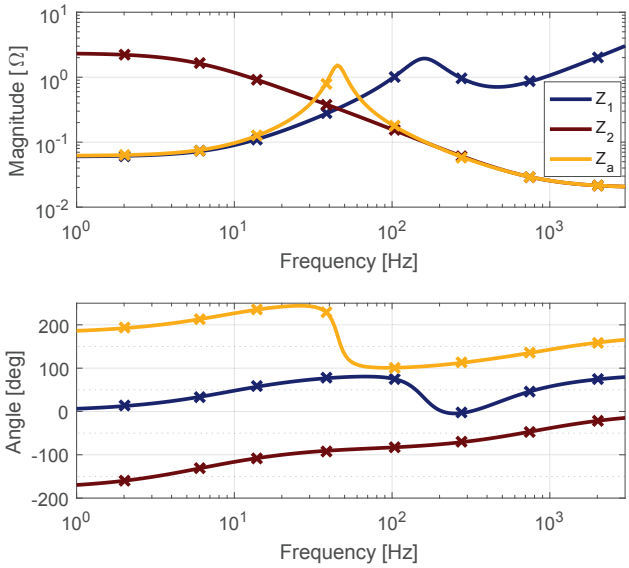

Fig. 8: Impedance plots obtained from the DC case system. 'x' represents the simulated values at f_{tab} (17), while the solid lines represent Vector Fitting

lower impedance than the capacitive path through the CPL.

D. Eigenvalue comparison

The next and final step in the stability analysis is to apply Vector Fitting (VF) to estimate the system state-space model, and to evaluate the eigenvalues of the matrix A. The input to VF is the set of simulated values for Z_a along with the frequency vector f_{tab} (17).

The VF directly outputs the state-space model and eigenvalues based on the sampled values of apparent impedance. The estimated (apparent) eigenvalues are presented in Table II. The difference between apparent eigenvalues and the analytical ones is less than 0.01 %. The eigenvalues are visualized in a plot in Fig. 9. The most critical eigenvalue has an imaginary

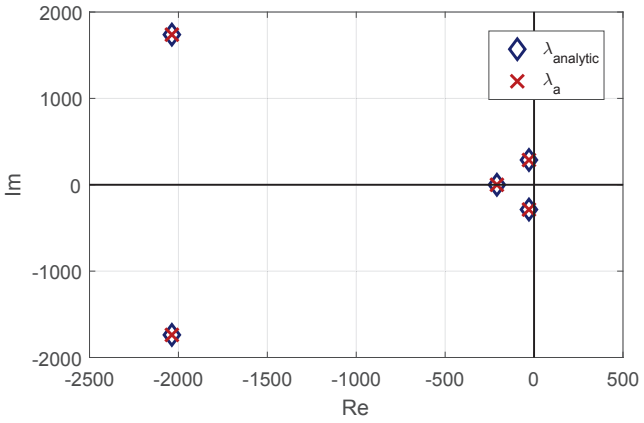

Fig. 9: Comparison of analytical and apparent eigenvalues for the DC-case (Table II)

part equal to 282.8, which is equivalent to an oscillation frequency of $\frac{282.8}{2\pi} = 45.0$ *Hz*. This is the same frequency as the apparent impedance resonances in Fig. 8.

In general, a resonant point in the apparent impedance plot will have an equivalent eigenvalue with poor damping ratio ζ. That is, a low ratio between real and imaginary parts.

TABLE II: Comparison of analytical eigenvalues with the apparent eigenvalues λ_a obtained at the DC case system. ζ: damping ratio, f: oscillation frequency

$\lambda_{analytic}$	λ_a	ζ	f [Hz]
$-30.39 \pm j282.8$	$-30.37 \pm j282.6$	0.107	45
$-2039 \pm j1743$	$-2039 \pm j1743$	0.76	277
-208.7	-208.7	1	0

VII. AC THREE-PHASE CASE STUDY EXAMPLE

A three-phase case has been defined in Fig. 10. This is a grid-connected Voltage Source Converter (VSC) equipped with *dq*-domain current control. A Phase Lock Loop (PLL) is used to synchronize with the grid, and it also includes an output LC-filter. The DC-link voltage is assumed constant. The grid is represented by a Thevenin equivalent. This is a relatively simple model with 16 state variables, and it is considered suitable for testing the apparent impedance method for three-phase systems. The analytic state-space model has been derived in Appendix A along with the parameter values. The current controller and PLL are tuned based on the principles in [24]. The current controller bandwidth is set to 200 rad/s, while the PLL bandwidth is set to 10 rad/s. When deriving the small-signal model, an equivalent second-order PWM delay transfer function is used to represent the effect of modulation and switching. T_c is the time delay parameter. The time delay can be model by several other techniques as well, e.g. by Pade approximation or Taylor series.

The apparent impedance matrix is extracted from simulation by the methodology in Fig. 3. The resulting impedance matrix is presented in Fig. 11. The crosses represent simulated frequencies, while the solid lines are the fitted results from the Matrix Fitting method. It is difficult to accurately interpret

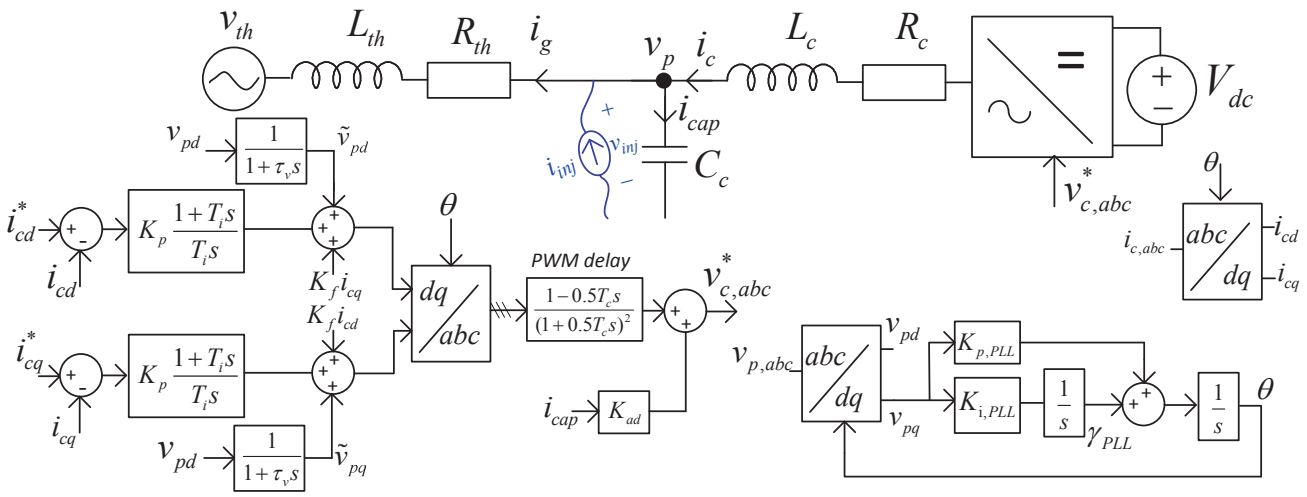

Fig. 10: Schematic of three-phase case-study system, including the injection source (i_{inj})

the impedance matrix by visual inspection, but a few resonance frequencies can be identified by inspecting the matrix elements individually. One at ≈ 15 Hz and one at ≈ 600 Hz.

Based on the estimated impedance crosses from Fig. 11 the Matrix Fitting routine will approximate a state-space model with associated eigenvalues. Average converter model is used during this simulation, and the simulation model is then based on the same equations as the analytical state-space model. These eigenvalues are plotted in Fig. 12, along with the analytical eigenvalues derived from (20). The match is very good for all 16 eigenvalues. Two small differences exist: The eigenvalue pair at -5932 ± 150.6 is estimated as a single eigenvalue at -5451, while the eigenvalue pair at $-20.08 \pm j2.398$ is estimated as a real pair at $-21.04 \quad \& \quad -18.89$. Both of these pairs have very low imaginary part, hence the practical implication of this estimation inaccuracy is negligible. The eigenvalues are also presented in Table III, along with their damping ratios and oscillation frequencies. The eigenvalues with lowest damping ratio have imaginary parts corresponding to 22.1, 588 and 704 Hz. These frequencies are the same as the resonant peaks in the impedance plot (Figure 11). The eigenvalues at 588 and 704 Hz appear as a combined resonance frequency at ≈ 670 Hz in the impedance plot. The close relation between eigenvalue imaginary parts and apparent impedance resonances can be explained by considering the impedance matrix on pole-residue form as discussed in Appendix D.

TABLE III: Comparison of analytical eigenvalues with the apparent eigenvalues in the three-phase case

$\lambda_{analytic}$	λ_a	ζ	f [Hz]
$-10.12 \pm j9.799$	$-10.32 \pm j9.698$	0.718	1.556
$-20.07 \pm j2.398$	$-21.04 \quad \& -18.89$	0.992	0.381
$-12.00 \pm j139.1$	$-11.75 \pm j139.0$	0.086	22
$-238.6 \pm j320.7$	$-237.8 \pm j320.8$	0.597	51
$-2093 \pm j811.8$	-2089.1 ± 824.4	0.932	129
$-981.1 \pm j3698$	$-977.6 \pm j3705$	0.256	588
$-1132 \pm j4423$	$-1128 \pm j4431$	0.248	703
$-5932 \pm j150.6$	-5451	1.00	24

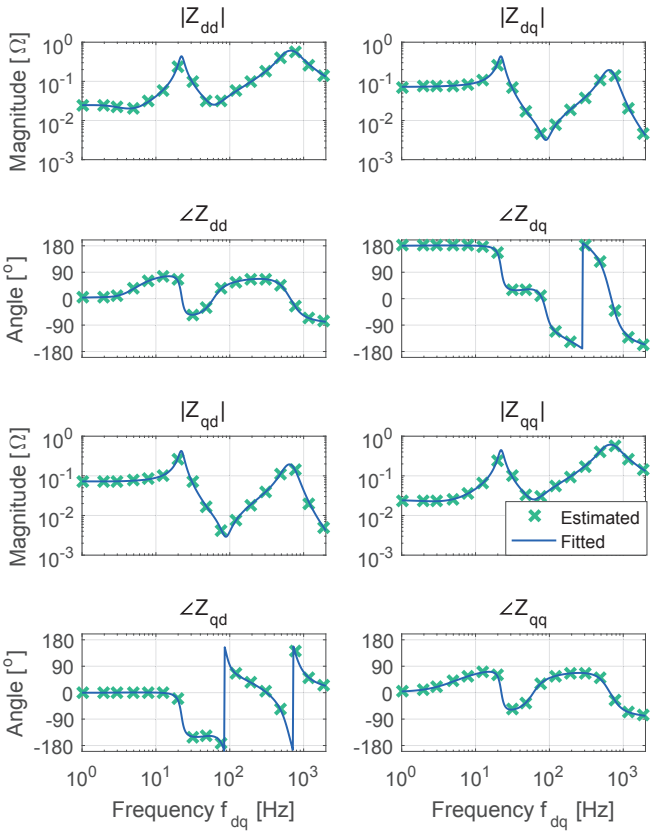

Fig. 11: Apparent impedance $\mathbf{Z}_a$ for the three-phase case. 'x' represents the simulated values, while the solid lines represent Matrix Fitting

VIII. Sensitivity analysis including unstable conditions (AC case)

The methodology presented in Fig. 3 is only able to analyze the system in stable conditions. This is due to the fact that a frequency sweep is only applicable to a stable system. However, the concept of apparent impedance analysis is also

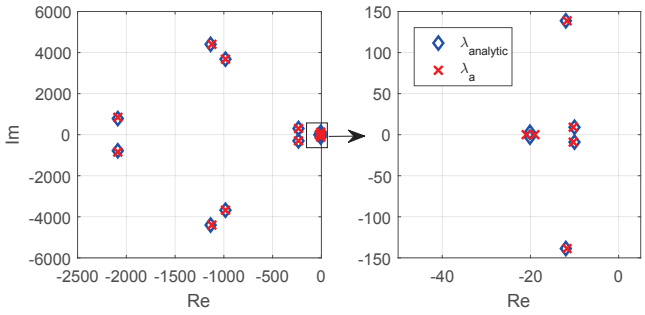

Fig. 12: Comparison of analytical and apparent eigenvalues for the three-phase case. Left: full overview, right: zoomed close to origin

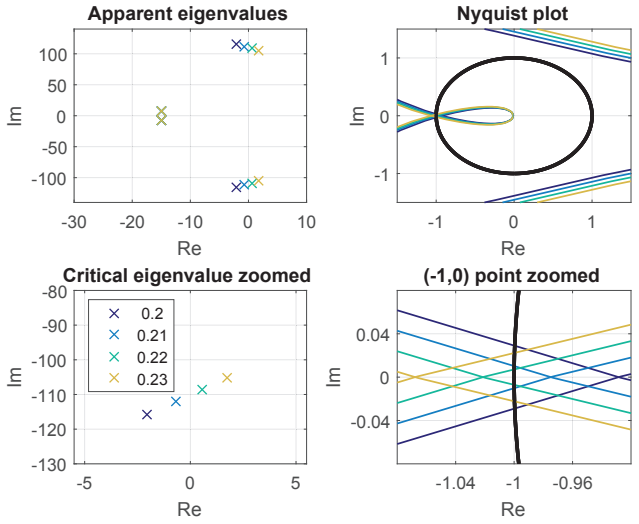

Fig. 13: Nyquist plot and apparent eigenvalue plot for varying grid impedance. Lower subplots represent a close-up of the upper plots.

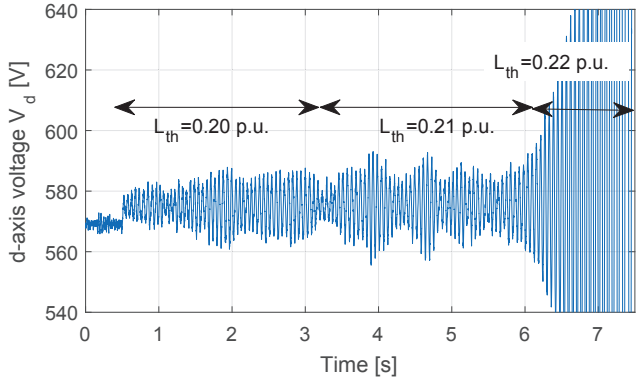

Fig. 14: Time-domain simulation (with switching converter model) verifying the stability analysis in Fig. 13

applicable to unstable conditions if some parts of the system is represented with either analytical or numerical data obtained from another source than the frequency sweep. It is also possible to completely avoid the sweep if the subsystem impedance data is known from other sources. The apparent impedance is calculated as the parallel connection of subsystem impedance by utilizing (7). In the following example the grid inductance is gradually increased until the stability limit is reached (and beyond). The apparent eigenvalues are then compared with the Nyquist plot obtained by using the Generalized Nyquist Criterion [25].

The main assumption in this example is that the converter impedance matrix does not change when the grid inductance changes. Then, this matrix is established once, and the apparent impedance matrix can be calculated for any grid impedance as the parallel connection of converter and grid impedance matrices (7) without running additional frequency sweeps. This assumption is only 100 % accurate if the converter operates in no-load condition. Otherwise, the interface point voltage will change due to increased grid impedance and its associated voltage drop, and this will change the converter impedance. If this effect is significant, additional sweeps need to be performed during the sensitivity analysis.

Fig. 13 shows some of the apparent eigenvalues as well as the Nyquist plots for four grid inductance values: $L_{th} = [0.20, 0.21, 0.22, 0.23]$ p.u. $= [0.303, 0.318, 0.333, 0.345]$ mH. The values are selected to give marginally stable and unstable conditions. It is seen that the stability conclusion is identical with the eigenvalues and the Nyquist plot, as instability is predicted when the grid inductance is 0.21 and 0.22 p.u..

A time-domain validation of this analysis is presented in Fig. 14. Note that a switching converter model is used for for this investigation, and therefore the waveforms are not smooth in the stable cases. The grid inductance is changed in the same steps, and it is observed whether the system is stable or unstable. The d-axis voltage is selected as the observed state variable, and it is clear that the system is unstable when L_{th} is 0.22 and 0.23 p.u.. This validates the stability analysis in Fig. 13. Even though the time-domain simulation in Fig. 14 is using a switching converter model, instability occurs at the same grid impedance as the apparent impedance analysis which is based on average converter model. This is explained from the fact that a first-order time delay is sufficient to analyze this specific instability issue. It is expected that stability issues at higher frequencies could require a more advanced representation of switching and modulation.

IX. Discussion and Further Work

In this section, the applicability of the method is dicsussed with respect to the following questions:

1) How large scale and complex systems can be analyzed with the apparent impedance method?
2) Can meshed systems be analyzed?
3) Can switching converter models be used?
4) Can the method be applied in experimental setups?
5) How will the method tackle unbalanced systems?

In principle, there is no upper limit on the number of state variables in the system to be analyzed. Still, it will clearly be hard to identify accurately all eigenvalues in a system with several thousand state variables. It is hard to give specific guidelines on how large systems that can be analyzed, but

it is suggested that the method can be used for all systems where conventional impedance-based analysis is used. This claim is justified by the fact that the same information is needed by both methods. Hence, the method is applicable to large systems, but dynamics that are not observable at the interface point may be overlooked. By performing the analysis in different injection locations, this problem can be overcome.

The hypothesis is that the method would work also for meshed systems, since it is not strictly required to define a source or load subsystem (only the apparent impedance). However, the analytical proof behind this hypothesis has not been derived at present. This will be investigated in further work.

The present paper uses average converter models in order to have a time invariant simulation model. This enables the accurate match with the eigenvalues from the analytical model. Furthermore, system-level stability analysis is normally conducted with average models, regardless of technique. The exception is when the frequency range of the stability issues of interest approaches the switching frequency. In this case, the method is considered less accurate.

Experimental setups for impedance-based stability analysis have demonstrated high accuracy in previous work, e.g. [15] [17]. Assuming that an impedance measurement system with high accuracy is available, the vector and matrix fitting algorithms will also estimate accurately the system state-space model. An important question to clarify is how the fitting step will be influenced by inaccuracies in the impedance measurement.

An unbalanced system will result in a time variant *dq*-domain model. In other words, the system cannot be modeled accurately with a *dq*-domain impedance matrix. In this case, another modeling domain is required, for instance the Harmonic State Space (HSS) [26]. By defining the apparent impedance in the HSS, it is expected that effects such as unbalances and power electronic switching can be captured accurately. The drawback of this extension is a more complicated procedure for impedance measurement. These investigations are left for further work.

X. Conclusions

The apparent impedance stability analysis method has been introduced and defined in this paper for DC and three-phase power systems. It has been shown that the apparent impedance can be used to estimate the eigenvalues of the system based on injection and measurements in a single point. The eigenvalues are directly obtained by applying a system identification algorithm to the measured set of apparent impedances. The method is proposed as an extension to well established impedance-based analysis based on source and load impedance models, and will provide additional information. Another application of the method is to validate analytically derived state-space models.

The case studies illustrate that the method is able to accurately identify the eigenvalues in both DC- and three-phase power systems. Further work needs to evaluate the robustness of the method in case of larger and more complex systems. A possible challenge when analyzing large system is that pole-zero cancellation inside one of the subsystems can occur. Then, the corresponding eigenvalues cannot be identified from the injection point unless the analysis is performed at multiple locations.

Acknowledgment

The authors would like to thank Dr. Bjørn Gustavsen at SINTEF Energy Research for developing the dedicated version of the Matrix Fitting routine that was used in this paper.

References

[1] R. D. Middlebrook, "Input filter considerations in design and application of switching regulators," in *IEEE Industry Applications Society Annual Meeting*, 1976.

[2] M. Belkhayat, *Stability criteria for AC power systems with regulated loads*. Purdue University, 1997.

[3] J. Sun, "Small-signal methods for ac distributed power systems;a review," *Power Electronics, IEEE Transactions on*, vol. 24, no. 11, pp. 2545–2554, Nov 2009.

[4] B. Gustavsen and A. Semlyen, "Rational approximation of frequency domain responses by vector fitting," *Power Delivery, IEEE Transactions on*, vol. 14, no. 3, pp. 1052–1061, Jul 1999.

[5] A. Rygg, M. Amin, M. Molinas, and B. Gustavsen, "Apparent impedance analysis: A new method for power system stability analysis," in *2016 IEEE 17th Workshop on Control and Modeling for Power Electronics (COMPEL)*, June 2016, pp. 1–7.

[6] F. Katiraei, M. R. Iravani, and P. W. Lehn, "Small-signal dynamic model of a micro-grid including conventional and electronically interfaced distributed resources," *IET Generation, Transmission Distribution*, vol. 1, no. 3, pp. 369–378, May 2007.

[7] N. Bottrell, M. Prodanovic, and T. C. Green, "Dynamic stability of a microgrid with an active load," *IEEE Transactions on Power Electronics*, vol. 28, no. 11, pp. 5107–5119, Nov 2013.

[8] S. D'Arco, J. A. Suul, and O. B. Fosso, "Automatic tuning of cascaded controllers for power converters using eigenvalue parametric sensitivities," *IEEE Transactions on Industry Applications*, vol. 51, no. 2, pp. 1743–1753, March 2015.

[9] S. Hiti, V. Vlatkovic, D. Borojevic, and F. C. Y. Lee, "A new control algorithm for three-phase pwm buck rectifier with input displacement factor compensation," *IEEE Transactions on Power Electronics*, vol. 9, no. 2, pp. 173–180, Mar 1994.

[10] S. Hiti, D. Boroyevich, and C. Cuadros, "Small-signal modeling and control of three-phase pwm converters," in *Proceedings of 1994 IEEE Industry Applications Society Annual Meeting*, Oct 1994, pp. 1143–1150 vol.2.

[11] K. D. T. Ngo, "Low frequency characterization of pwm converters," *IEEE Transactions on Power Electronics*, vol. PE-1, no. 4, pp. 223–230, Oct 1986.

[12] Z. Yao, P. G. Therond, and B. Davat, "Frequency characteristics of ac power systems," in *Proceeding of IFAC 1993 World Congress*, vol. 5-443, July 1993.

[13] R. Burgos, D. Boroyevich, F. Wang, K. Karimi, and G. Francis, "On the ac stability of high power factor three-phase rectifiers," in *Energy Conversion Congress and Exposition (ECCE), 2010 IEEE*. IEEE, 2010, pp. 2047–2054.

[14] B. Wen, D. Dong, D. Boroyevich, R. Burgos, P. Mattavelli, and Z. Shen, "Impedance-based analysis of grid-synchronization stability for three-phase paralleled converters," *Power Electronics, IEEE Transactions on*, vol. PP, no. 99, pp. 1–1, 2015.

[15] G. Francis, R. Burgos, D. Boroyevich, F. Wang, and K. Karimi, "An algorithm and implementation system for measuring impedance in the d-q domain," in *Energy Conversion Congress and Exposition (ECCE), 2011 IEEE*, Sept 2011, pp. 3221–3228.

[16] Y. Familiant, J. Huang, K. Corzine, and M. Belkhayat, "New techniques for measuring impedance characteristics of three-phase ac power systems," *Power Electronics, IEEE Transactions on*, vol. 24, no. 7, pp. 1802–1810, July 2009.

[17] M. Cespedes and J. Sun, "Three-phase impedance measurement for system stability analysis," in *Control and Modeling for Power Electronics (COMPEL), 2013 IEEE 14th Workshop on*. IEEE, 2013, pp. 1–6.

[18] B. Gustavsen, "Improving the pole relocating properties of vector fitting," *Power Delivery, IEEE Transactions on*, vol. 21, no. 3, pp. 1587–1592, July 2006.

[19] D. Deschrijver, M. Mrozowski, T. Dhaene, and D. De Zutter, "Macromodeling of multiport systems using a fast implementation of the vector fitting method," *Microwave and Wireless Components Letters, IEEE*, vol. 18, no. 6, pp. 383–385, June 2008.

[20] "The vector fitting web page," https://www.sintef.no/projectweb/vectfit/, accessed: 2016-02-19.

[21] L. Harnefors, X. Wang, A. G. Yepes, and F. Blaabjerg, "Passivity-based stability assessment of grid-connected vscs;an overview," *IEEE Journal of Emerging and Selected Topics in Power Electronics*, vol. 4, no. 1, pp. 116–125, March 2016.

[22] L. Harnefors, R. Finger, X. Wang, H. Bai, and F. Blaabjerg, "Vsc input-admittance modeling and analysis above the nyquist frequency for passivity-based stability assessment," *IEEE Transactions on Industrial Electronics*, vol. PP, no. 99, pp. 1–1, 2017.

[23] X. Wang, F. Blaabjerg, and P. C. Loh, "Passivity-based stability analysis and damping injection for multi-paralleled voltage-source converters with lcl filters," *IEEE Transactions on Power Electronics*, vol. PP, no. 99, pp. 1–1, 2017.

[24] L. Harnefors, M. Bongiorno, and S. Lundberg, "Input-admittance calculation and shaping for controlled voltage-source converters," *Industrial Electronics, IEEE Transactions on*, vol. 54, no. 6, pp. 3323–3334, Dec 2007.

[25] C. Desoer and Y.-T. Wang, "On the generalized nyquist stability criterion," *Automatic Control, IEEE Transactions on*, vol. 25, no. 2, pp. 187–196, Apr 1980.

[26] J. Kwon, X. Wang, F. Blaabjerg, C. L. Bak, V. S. Sularea, and C. Busca, "Harmonic interaction analysis in grid-connected converter using harmonic state space (hss) modeling," *IEEE Transactions on Power Electronics*, vol. PP, no. 99, pp. 1–1, 2016.

[27] S. Grivet-Talocia and B. Gustavsen, *Passive macromodeling: Theory and applications*. John Wiley & Sons, 2015, vol. 239.

APPENDIX

A. Analytic state-space model of AC-system

The state-space model of the three-phase system in Fig. 10 has been derived in (20), while the parameter values and operation point is given in Table IV. The state-space model is without any elements B, C, D and E since only the eigenvalues of matrix A are relevant for the stability analysis. Note that superscript 0 indicates the steady-state operation point. Superscript *s* and *c* in the state variables indicate system and converter reference frame, respectively, as defined in [14]. The state variables and parameters can be identified in Fig. 10. Note specifically that γ_d^c and γ_q^c are the output of the integrators in the current controller. The four states needed to model the second order PWM delay are defined as $x_{pwm1,d}, x_{pwm1,q}, x_{pwm2,d}, x_{pwm2,q}$ in the equation below.

The symbols are explained as follows, see also Fig. 10. V_{DC} is the converter DC-link voltage, V_{th}, R_{th} and L_{th} represents the grid Thevenin equivalent. L_c, C_c and R_c represent the filter on the converter AC-terminals. K_p and T_i is the current PI-controller parameters. τ_v is the voltage feed-forward filter time constant. $K_{p,PLL}$ and $K_{i,PLL}$ is the PLL PI-controller. T_c is the combined switching, modulation and ADC time delay. K_{ad} is the active damping gain. ω_1 is the fundamental frequency, while f_{sw} is the switching frequency. The converter operation point is given by $I_{cd}^0, I_{cq}^0, V_{pd}^0, V_{pq}^0$.

TABLE IV: Parameter data applied in the simulation model

Parameter	Value	Parameter	Value
V_{DC}	1240 V	V_{th}	690 V (LL-RMS)
R_{th}	23.8 $m\Omega$	L_{th}	0.227 mH
C_c	0.669 mF	L_c	0.152 mH
R_c	9.52 $m\Omega$	K_p	0.0757 V/A
T_i	4.0 ms	τ_v	50 ms.
$K_{p,PLL}$	0.0355 rad/(Vs)	$K_{i,PLL}$	0.355 rad/(Vs^2)
T_c	0.0005 s	K_{ad}	0.33 V/A
ω_1	100π rad/s	I_{cd}^0	0 A
I_{cq}^0	0 A	V_{pd}^0	574 V
V_{pq}^0	574 V	f_{sw}	2 kHz

B. Pole-residue representation of transfer functions and matrices

The vector and matrix fitting algorithms are based on pole-residue representation of transfer functions [27]. For the SISO-case, this can be viewed as the partial fraction expansion of a real transfer function $H(s)$:

$$\begin{aligned} H(s) &= \frac{b_m s^m + b_{m-1}s^{m-1} + ... + b_1 s + b_0}{a_n s^n + a_{n-1}s^{n-1} + ... + a_1 s + a_0} \\ &= \frac{r_1}{s-\lambda_1} + \frac{r_2}{s-\lambda_2} + ... + \frac{r_n}{s-\lambda_n} + D + sE \end{aligned} \tag{18}$$

where r_i is the residue corresponding to eigenvalue (or pole) λ_i. The parameter D is non-zero whenever $m \geq n$, while E is non-zero whenever $m > n$. Additional terms such as s^2F may be needed if the transfer function satisfies $m > n+1$, but this is a very rare property in actual systems.

In the matrix fitting toolbox (MIMO-case), the residue r_i is replaced by a residue matrix $\mathbf{R}_i$ as follows:

$$\mathbf{H}(s) = \frac{\mathbf{R}_1}{s-\lambda_1} + \frac{\mathbf{R}_2}{s-\lambda_2} + ... + \frac{\mathbf{R}_n}{s-\lambda_n} + \mathbf{D} + s\mathbf{E} \tag{19}$$

As seen in (19) and elaborated in [27], each element in the transfer matrix $\mathbf{H}(s)$ is fitted to the same set of eigenvalues. It is the residue matrices, as well as $\mathbf{D}$ and $\mathbf{E}$ that gives the difference between different elements in the transfer matrix $\mathbf{H}(s)$.

If the system has a poorly damped eigenvalue $\lambda_i = \alpha_i + j\omega_i$, the corresponding fraction $\frac{1}{s-\lambda_i}$ will become very large at $s = j\omega_i$. For the SISO-case, this will give a resonance peak in the transfer function at ω_i. For the MIMO-case, it is clear from (19) that all elements in the transfer matrix $\mathbf{H}(s)$ will have a resonance peak at this frequency. The only exception is when a certain element of the residue matrix $\mathbf{R}_i$ is either zero or very small.

C. Additional details on the vector fitting method

The state-space representation in (5) can also be expressed as a sum of partial fractions:

$$\begin{aligned} Z_a(s) &= C\left(sI - A\right)^{-1} B + D + sE \\ Z_a(s) &= \sum_{i=1}^{n} \frac{R_i}{s-\lambda_i} + D + sE \end{aligned} \tag{21}$$

where λ_i is the i'th pole and R_i is the i'th *residue*. It is seen that the residues measures of the observability of the i'th eigenvalue in the transfer function $Z_a(s)$. The ratio $\left|\frac{R_i}{\lambda_i}\right|$ is therefore proposed in section V-A as the parameter for identifying if an eigenvalue is significant or not.

If the state-space model is expressed by a diagonal *A*-matrix, the residues can be related to vectors *B* and *C* as:

$$R_i = b_i c_i \tag{22}$$

where b_i is the i'th element of the vector *B*, and c_i is the i'th element of the vector *C*.

$$s\mathbf{x} = A\mathbf{x}$$

$$\mathbf{x} = [x_{pwm1,d}, x_{pwm1,q}, x_{pwm2,d}, x_{pwm2,q}, i^s_{cd}, i^s_{cq}, v^s_{pd}, v^s_{pq}, \tilde{v}^c_{pd}, \tilde{v}^c_{pq}, i^s_{gd}, i^s_{gq}, \gamma^c_d, \gamma^c_q, \gamma_{PLL}, \theta]^T$$

$$A = \begin{bmatrix}
-\frac{4}{T_c} & \omega_1 & -\frac{4}{T_c^2} & 0 & -\frac{K_pV_{dc}}{2T_c} & -\frac{K_f}{T_c} & 0 & 0 & \frac{1}{T_c} & 0 & 0 & 0 & \frac{V_{dc}}{2T_c} & 0 & 0 & \alpha_1 \\
-\omega_1 & -\frac{4}{T_c} & 0 & -\frac{4}{T_c^2} & \frac{K_f}{T_c} & -\frac{K_pV_{dc}}{2T_c} & 0 & 0 & 0 & \frac{1}{T_c} & 0 & 0 & 0 & \frac{V_{dc}}{2T_c} & 0 & \alpha_2 \\
1 & 0 & 0 & \omega_1 & 0 & 0 & 0 & 0 & 0 & 0 & 0 & 0 & 0 & 0 & 0 & 0 \\
0 & 1 & -\omega_1 & 0 & 0 & 0 & 0 & 0 & 0 & 0 & 0 & 0 & 0 & 0 & 0 & 0 \\
-\frac{2}{L_c} & 0 & \frac{4}{T_cL_c} & 0 & -\frac{K_{ad}+R_c}{L_c} & \omega_1 & -\frac{1}{L_c} & 0 & 0 & 0 & \frac{K_{ad}}{L_c} & 0 & 0 & 0 & 0 & -\frac{V^0_{cq}}{L_c} \\
0 & -\frac{2}{L_c} & 0 & \frac{4}{T_cL_c} & -\omega_1 & -\frac{K_{ad}+R_c}{L_c} & 0 & -\frac{1}{L_c} & 0 & 0 & 0 & \frac{K_{ad}}{L_c} & 0 & 0 & 0 & \frac{V^0_{cd}}{L_c} \\
0 & 0 & 0 & 0 & \frac{1}{C_c} & 0 & 0 & \omega_1 & 0 & 0 & -\frac{1}{C_C} & 0 & 0 & 0 & 0 & 0 \\
0 & 0 & 0 & 0 & 0 & \frac{1}{C_c} & -\omega_1 & 0 & 0 & 0 & 0 & -\frac{1}{C_c} & 0 & 0 & 0 & 0 \\
0 & 0 & 0 & 0 & 0 & 0 & \frac{1}{\tau_v} & 0 & -\frac{1}{\tau_v} & 0 & 0 & 0 & 0 & 0 & 0 & \frac{V^0_{pq}}{\tau_v} \\
0 & 0 & 0 & 0 & 0 & 0 & 0 & \frac{1}{\tau_v} & 0 & -\frac{1}{\tau_v} & 0 & 0 & 0 & 0 & 0 & -\frac{V^0_{pd}}{\tau_v} \\
0 & 0 & 0 & 0 & 0 & 0 & \frac{1}{L_{th}} & 0 & 0 & 0 & -\frac{R_{th}}{L_{th}} & \omega_1 & 0 & 0 & 0 & 0 \\
0 & 0 & 0 & 0 & 0 & 0 & 0 & \frac{1}{L_{th}} & 0 & 0 & -\omega_1 & -\frac{R_{th}}{L_{th}} & 0 & 0 & 0 & 0 \\
0 & 0 & 0 & 0 & -\frac{K_p}{T_i} & 0 & 0 & 0 & 0 & 0 & 0 & 0 & 0 & 0 & 0 & -\frac{I^0_{cq}K_p}{T_i} \\
0 & 0 & 0 & 0 & 0 & -\frac{K_p}{T_i} & 0 & 0 & 0 & 0 & 0 & 0 & 0 & 0 & 0 & \frac{I^0_{cd}K_p}{T_i} \\
0 & 0 & 0 & 0 & 0 & 0 & 0 & K_{i,PLL} & 0 & 0 & 0 & 0 & 0 & 0 & 0 & \alpha_3 \\
0 & 0 & 0 & 0 & 0 & 0 & 0 & K_{p,PLL} & 0 & 0 & 0 & 0 & 0 & 0 & 1 & \alpha_4
\end{bmatrix}$$

$$\alpha_1 = \frac{-\frac{1}{2}I^0_{cq}K_pV_{dc} + K_fI^0_{cd}}{T_c}$$

$$\alpha_2 = \frac{\frac{1}{2}I^0_{cd}K_pV_{dc} + K_fI^0_{cq}}{T_c}$$

$$\alpha_3 = -K_{i,PLL}V^0_{pd}$$

$$\alpha_4 = -K_{p,PLL}V^0_{pd} \tag{20}$$

D. Additional details on the matrix fitting method

The equations from appendix C are extended to MIMO-systems in order to be applicable to the matrix fitting method. Assuming the 2x2 *dq* impedance matrix $\mathbf{Z}_{dq}$ is the transfer function yields:

$$\begin{aligned}\mathbf{Z}_{dq}(s) &= \begin{bmatrix} Z_{dd}(s) & Z_{dq}(s) \\ Z_{qd}(s) & Z_{qq}(s) \end{bmatrix} = \mathbf{C}\left(s\mathbf{I} - \mathbf{A}\right)^{-1}\mathbf{B} + \mathbf{D} + s\mathbf{E} \\ &= \sum_{i=1}^{n} \frac{\mathbf{R}_i}{s - \lambda_i} + \mathbf{D} + s\mathbf{E} \end{aligned} \tag{23}$$

where $\mathbf{R}_i$ is the 2x2 residue matrix corresponding to the i'th eigenvalue λ_i. When defining a norm to evaluate if an eigenvalue is *significant* or not, the following condition is proposed:

$$\frac{||\mathbf{R}_i||_2}{|\lambda_i|} > 10^{-4} \tag{24}$$

where $||(\cdot)||_2$ is the *2-norm* of a matrix (other matrix norms can also be applied).

E. Definition of a passive system

The definition from [27] is adopted in this work. A passive system is defined as a system that is not able to generate energy on its own. Mathematically this can be formulated by representing the system with transfer matrix $\mathbf{H}(s)$ (e.g the 2x2 impedance matrix $\mathbf{Z}_{dq}(s)$). If the system is passive, the following condition holds:

$$\lambda_i \geq 0 \qquad \forall \lambda_i \in (\mathbf{H}(j\omega) + \mathbf{H}(j\omega)^H) \qquad \omega \in \mathbb{R} \tag{25}$$

Where $\mathbf{H}(j\omega)^H$ is the conjugate transpose (Hermitian transpose) of $\mathbf{H}(j\omega)$. The condition is that all eigenvalues of $\mathbf{H}(j\omega)+\mathbf{H}(j\omega)^H$ are positive for all frequencies ω.

For a single-input-single-output system $H(j\omega)$, the condition is simplified to requiring $-90^o \leq \angle H(j\omega) \leq 90^o$. This is a more intuitive definition of passivity, since a negative real part of the terminal characteristic is associated with production of energy.

Atle Rygg received the MSc degree in Electrical Engineering from the Norwegian University of Science and Technology (NTNU) in 2011. From 2011 to 2015 he was a research scientist at SINTEF Energy Research in the field of power electronics. He is currently pursuing his PhD-degree at department of engineering cybernetics at NTNU. His topic or research is impedance based stability analysis of power electronic systems, where the aim is to contribute to the fundamental understanding in this family of methods.

Marta Molinas (M'94) received the Diploma degree in electromechanical engineering from the National University of Asuncion, Asuncion, Paraguay, in 1992; the Master of Engineering degree from Ryukyu University, Japan, in 1997; and the Doctor of Engineering degree from the Tokyo Institute of Technology, Tokyo, Japan, in 2000. She was a Guest Researcher with the University of Padova, Padova, Italy, during 1998. From 2004 to 2007, she was a Postdoctoral Researcher with the Norwegian University of Science and Technology (NTNU) and from 2008-2014 she has been professor at the Department of Electric Power Engineering at the same university. She is currently Professor at the Department of Engineering Cybernetics, NTNU. Her research interests include stability of power electronics systems, harmonics, instantaneous frequency, and non-stationary signals from the human and the machine. She is Associate Editor for the IEEE Journal JESTPE, IEEE PELS Transactions and Editor of the IEEE Transactions on Energy Conversion. Dr. Molinas has been an AdCom Member of the IEEE Power Electronics Society from 2009 to 2011.